Issues in the inverse modeling of a single ring infiltration experiment

Michal Kuraz[a], Lukas Jacka[a], Johanna Ruth Bloecher[a], Matej Leps[b]

[a] *Czech University of Life Sciences Prague, Faculty of Environmental Sciences, Department of Water Resources and Environmental Modeling*
[b] *Czech Technical University in Prague, Faculty of Civil Engineering, Department of Mechanics*

Abstract

This contribution addresses issues in identification of ~~the~~ soil hydraulic properties (SHP) obtained from inverse modeling of a single ring (SR) infiltration experiment. The SR experimental data were obtained from series of in situ experiments conducted on a mountainous podzolic soil profile. The main purpose of this inverse model was to evaluate the SHP of the top soil layer described ~~here~~ by the van Genuchten's (VG) parameters, and to answer the question whether the well-known SR experiment is robust enough to provide an estimate of these properties.

The top soil layer SHP are very difficult to measure directly, since the thickness of the top soil layer is often much lower than the depth required to embed the SR or Guelph permeameter device or to obtain undisturbed samples for ~~further~~ laboratory experiments.

The main issue, which is addressed in this contribution, is the uniqueness of the Richards equation based inverse model of SR experiment with van Genuchten's constitutive function for the retention curve and Mualem's function for the unsaturated hydraulic conductivity. We tried to answer the question whether is it possible to characterize the unsteady part of the SR infiltration experiment with a unique set of parameters representing SHP, and whether ~~are~~ all ~~of~~ ~~these~~ parameters vulnerable ~~with~~ ~~the~~ non-uniqueness. The sophisticated differential evolution based algorithm SADE Ibrahimbegović et al. (2004), which stores all identified local optima in memory was used for this analyses.

Further the issues in assigning the initial and boundary condition setup, the influence of spatial and temporal discretization on the values of the identified SHP, and the convergence issues with the Richards equation nonlinear operator during automatic calibration procedure are also mentioned here.

Keywords: soil hydraulic properties, inverse modeling of the Richards equation, FEM approximation of the Richards equation, differential evolution, application of dd-adaptivity algorithm, computational hydrology, computational soil science

1. Introduction

Soil hydraulic properties (hereafter SHP), such as saturated hydraulic conductivity, residual and saturated weater content, and typically van Genuchten (hereafter VG) parameters (van Genuchten, 1980) governing the retention curve and the unsaturated hydraulic conductivity, are important for many hydrological models and engineering applications. The mountainous podzolic soil evaluated here is typical for the source areas of many major rivers in the Central European region. The top layer of the soil plays a key role in the rainfall-runoff process, because it is the top-soil that separates the rainfall into surface runoff and subsurface runoff.

Due to the rocks that are present and the dense root system of the covering vegetation, and due to the possible extension of the representative elementary volume, it is often impossible to collect undisturbed samples of top-soil for laboratory measurements in order to obtain the SHP parameters (Jačka et al., 2014). The SHP of the top-soil are therefore very difficult to measure directly (Fodor et al., 2011; Jačka et al., 2014).

In our study, the well-known single ring (hereafter SR) method was used to obtain experimental input data (cumulative infiltration) for inverse modeling. The SR infiltrometer is a widely accepted, simple, robust field method, which is able to measure infiltration process, which affects the entire soil profile including the top-soil, and can sample a relatively large volume (depending on the diameter of the ring) (Cheng et al., 2011; Reynolds, 2008a). The SR infiltration experiment is an in situ experiment, which does not require soil samples to be collected, so the porous medium is kept relatively undisturbed. With the widely-used ring diameter of 30 cm, the affected porous media is far more representative than any soil sample we were able to collect. The top-soil can also be measured (with some alteration of the surface) using other well-known field infiltration methods, e.g. the tension infiltrometer or the well permeameter (see (Angulo-Jaramillo et al., 2000; Reynolds, 2008b)).

The flow in a variably saturated porous medium is governed by the Richards equation (Richards, 1931) parametrized by SHP represented by the saturated hydraulic conductivity, the residual and saturated water content, and VG parameters. This model will abbreviated in this contribution as REVG.

Several studies compared REVG inverse modeling of tension infiltrometers (Verbist et al., 2009; Simunek et al., 1998; Ventrella et al., 2005; Schwartz and Evett, 2002; Ramos et al., 2006; Simunek et al., 1999; Rezaei et al., 2016). It states that the retention curves obtained from this inverse modeling using tension infiltrometer data are often not in ~~a~~ good agreement with laboratory experiments on undisturbed samples. In particular, the saturated water content obtained from an inverse model of REVG is typically distinctly

lower than the experimentally established value (~~see e.g.~~ (Simunek et al., 1998; Verbist et al., 2009)). There are various theories explaining this issue ~~as e.g.~~ the effect of hysteresis as a drying process in the laboratory differs from the wetting process in the field; the effect of entrapped air in the field (see e.g. (Fodor et al., 2011)), where the saturation may not fully correspond the pressure head, and an effect of macropores, which are excluded when a tension infiltrometer is used. ~~But~~ most importantly the soil samples, which are usually examined in the laboratory, are typically much smaller than the representative elementary volume (Scharnagl et al., 2011). But on the other hand several studies reported a close correspondence between the retention curve parameters obtained from laboratory experiments and from the REVG analyses (Ramos et al., 2006; Schwartz and Evett, 2002). ~~An~~ identification of SHP from transient infiltration experiment was a subject of numerous publications in past decades ~~already~~ (Inoue et al., 2000; Lassabatère et al., 2006; Kohne et al., 2006; Xu et al., 2012; Bagarello et al., 2017; Younes et al., 2017). Inoue et al. (2000) ~~already~~ reported a close correspondence between the SHP obtained from ~~the~~ inverse modeling of dynamic transient infiltration experiment with those obtained from steady-state laboratory experiment, where the uniqueness of his inverse model was preserved by considering the dynamically changing pressure head, water content and even tracer concentration.

The non-uniqueness of the REVG inverse model is ~~already~~ a very well-known issue, and has been described by a number of publications over the last decades (Kool et al., 1985; Mous, 1993; Hwang and Powers, 2003; Binley and Beven, 2003). **However, we have not succeeded in our search for more recent contributions in this field.** Mous (1993) defined criteria for model identifiability based on the sensitivity matrix rank, however numerical computation of sensitivity matrix, which is represented by derivatives of the objective function, often involves difficulties in maintaining truncation and also round-off errors. Binley and Beven (2003) demonstrated on real world case study of Sherwood Sandstone Aquifer that many different SHP parameters of macroscopic media representing the layered unsaturated zone provided acceptable simulations of the observed aquifer recharges. However, in this work the non-unique definition with the unknown residual and saturated water content was considered, despite Mous (1993) noticed that in case of an absence of the water content experimental data, the residual water content should be excluded from the identification. The definition of unique inverse function for identification of macroscopic media was treated in (Zou et al., 2001), where the recommended approach was to assemble the objective function from transient data of the capillary pressure and from the steady state water content data.

must be checked!!

And yet another challenging issue is the treatment of the nonlinear operator of the Richards equation. Binley and Beven (2003) reported that during their Monte Carlo simulations on wide ranges of SHPs values

56% of simulations were rejected, because of convergence problems. It wasn't mentioned in the paper explicitly, we can only suggest that these convergence issues originated from the nonlinear operator treatment – the outer iterations. It could be ~~easily~~ concluded, that if we use simple Picard method for the nonlinear operator, and we increase the iteration criterion (which is typically ~~a~~ so-called h or θ tolerance), we will obtain less accurate solution but we will also need less iterations for the Picard method. If we further increase the criterion we will end up with semi-implicit solution, where the constitutive functions in the Richards equation are evaluated from the previous time level solution – thus we will always need just a single outer iteration.

And so the following questions arise.

- Is it possible to approximate the unsteady SR experiment by REVG model, where the only unknown parameters represent the thin top-soil layer ~~SHP~~, by a unique set of parameters?
- If not are all ~~SHPs~~ parameters vulnarable with this non-uniqueness?
- Are the SHP parameters identified by inverse analyses of SR infiltration dependent on the treatment of the nonlinear operator of the Richards equation? Is there any benefit in using the accurate Newton or Picard iteration method (which can often lead to a slow convergence or even divergence of the REVG nonlinear operator), or can we obtain a reasonable estimate with just the semi-implicit scheme?

The aim of this paper is to answer these proposed issues. The inverse ~~modeling~~ problem applied here for evaluating these issues is a real world problem of identification of the SHP for top soil podzolic horizons of experimental catchment Modrava, Sumava National Park, Czech Republic. The SHP for the lower horizons were already described by various field and laboratory experiments and by data processing (e.g. pedotransfer functions, see Rosetta code (Schaap et al., 2001)), only the top soil SHP are difficult to obtain directly. Moreover, for this type of top soil layer it is even a very difficult to guess some estimates of its SHPs. However, the knowledge of the lower horizons should decrease the number of unknowns of this inverse problem. In addition to answering the given questions, which are nearly classical but not satisfactory resolved issues in this field of research, we will also try to address issues with initial and boundary condition setup for the approximation of SR infiltration process. And finally, the numerical issues originating from the convection term in the Richards equation representing the axisymmetric SR infiltration flux will be also discussed in this work.

2. Methodology

This section is divided into two distinct parts. The first part, section 2.1, is focused on assembling the experimental data, which were ~~later~~ used for ~~the~~ inverse modeling. In ~~this~~ section the site description, the reconstruction of the parameters of the SHPs for the lower profiles, and the processing of the experimental data is given. ~~This section also provides~~ a complete definition of the SHPs parameters – the solution of our inverse problem – ~~particularly~~ in the paragraph 2.1.2.

The second part of the methodology, section 2.2, covers the main topic of this paper – issues in the Richards equation based inverse model. The governing equation is given together with notes about the numerical stability of the convection dominant problems, since it is not always mentioned that diffusion type equation in cylindrical coordinates contains a first order derivative term, and so ~~the~~ numerical stability issues appear. A typical example of this vulnerable problem is the Richards equation ~~or the groundwater flow equation~~ for rotational symmetric problems, where the cylindrical coordinates enable reduction of the three-dimensional computational domain into a two-dimensional domain, which is a widely used approach. Further the issues in selecting an appropriate boundary conditions are discussed, since it is not always easy to find an agreement between the mathematical model setup and physical interpretation. Finally, the most important part, the construction of the objective function, and the methodology of the automatic calibration is given in this section.

2.1. Obtaining the input data for inverse modeling

2.1.1. Site description and assembling the experimental data

The study site is located in the Šumava National Park, and ~~has been~~ described in (Jačka et al., 2014). The location of the site in a map of Modrava 2 catchment is presented by Jačka et al. (2012). A haplic podzol with distinct soil horizons is dominant on this site. The mean depths of the podzolic horizons are as follows:

- organic horizon O and humus horizon Ah altogether (the top-soil) 7.5 cm,
- eluvial bleached horizon E 12.5 cm,
- spodic horizons Bhs and Bs 40 cm,
- highly conductive weathered bedrock C.

The average groundwater table level can be roughly estimated at -280 cm below the surface. Based on the soil texture analysis obtained from the hydrometer method; horizon E contains 1% clay ($< 2\mu$m), 20% silt (2μm – 0.05 mm), 79% sand (0.05 – 2 mm), and 32% gravel (> 2 mm); and the spodic horizons contain 7% clay, 32% silt, 61% sand, and 30% gravel. The bulk densities of the lower soil horizons are as follows: E 1.4 g.cm^{-3}; Bhs and Bs 1.3 g.cm^{-3}. The porosities of the lower horizons, estimated using the bulk density of the undisturbed soil samples and the mean density of the soil solid particles, are as follows: horizon E 46%, spodic horizons Bhs and Bs 47%. The porosities of the upper horizons (0 and Ah) were estimated only very roughly, due to possible disturbance of the samples (particularly dense roots and vegetation cover, which caused difficulties in sampling), and due to shrinkage of the samples during the drying process. The bulk density was estimated as 0.4 g.cm^{-3}, and the porosity was estimated as 85%. However the porosity of the upper horizon will be the subject of our parameter identification conducted here.

In order to obtain data for identifying the hydraulic parameters of the top-soil, a total of 22 SR infiltration experiments were performed. The experimental sites in our catchment were selected randomly. The minimal distance between infiltration sites was 1.5 m. All in situ experiments and sample collections were performed in August.

2.1.2. Soil hydraulic parameters

The soil hydraulic parameters (SHP) represent the hydrodynamic properties of porous media under variably saturated conditions.

In this work, the SHPs are considered to be the following:

- Parameters representing the van Genuchten retention curve model (van Genuchten, 1980), particularly α [L^{-1}] and n [-]. The van Genuchten parameter m was considered as $m = 1 - \frac{1}{n}$.
- Saturated water content θ_s [-]. Note that the residual water content θ_r [-] is neglected here, because together with the unknown saturated water content, the unknown residual water content can hardly lead to a unique solution of the inverse modeling. Unless we were able to conduct an accurate measurement of the water content during the experiment, which is often complicated. Especially, if we take into consideration, that it is much easier to measure the saturated water content after the experiment, than to measure the unsaturated water content and the pressure head during the experiment. However, as specified above, no exact saturated water content data of the top soil horizon were available.
- Saturated hydraulic conductivity K_s [$L.T^{-1}$].

- Specific storage S_s $[L^{-1}]$ – represents the linear elasticity of the porous medium. The specific storage in the unsaturated zone is often neglected. However, the effect of the elasticity of the top-soil during the infiltration experiment, which is typical with an abrupt development of hydraulic pressure, should also be included.

An evaluation of these parameters is the scope of this work. The focus will be given on the top soil layer, where this set of parameters will be identified by inverse analysis. The SHPs parameters of the lower layers ~~will be~~ obtained here using Guelph permeameter (GP) measurements and Rosetta pedotransfer functions (Schaap et al., 2001).

2.1.3. Obtaining SHP parameters for lower horizons

Guelph permeameter measurements (GP) were used for estimating the saturated hydraulic conductivity of the lower horizons. When evaluating horizon E, the measurements were performed in wells with depth ranging between 19 cm and 26 cm. For the spodic horizon the depth of the measurement wells ranged between 30 cm and 56 cm. The constant head GP method applied here is described in (Jačka et al., 2014).

A total of 28 GP experiments were conducted to estimate the saturated hydraulic conductivity of the E horizon. The representative saturated hydraulic conductivity for the E horizon was evaluated as $4.0{\times}10^{-6}$ m.s^{-1}.

A total 19 GP experiments were conducted to estimate the saturated hydraulic conductivity of the spodic horizon. The estimated geometric mean value is: $K_s = 1.5 \times 10^{-6}$ m.s^{-1}.

The saturated hydraulic conductivity of the weathered bedrock C was obtained as the geometric mean from 8 experiments performed using the GP method in wells from 68 to 130 cm in depth. The estimated mean geometric value is: $K_s = 8.5 \times 10^{-6}$ m.s^{-1}.

Representative parameters of the retention curves (for the eluvial horizon below the top-soil, spodic horizons and weathered bedrock) were estimated using the soil texture and the bulk density information and a neural network prediction (a type of pedo-transfer function) of Rosetta code, see (Schaap et al., 2001).

It is well known that pedotransfer functions work well for spodic and eluvial horizons characterized by high percentage of sand, without a distinct structure, and with a bulk density and porosity corresponding to a standard mineral soil. And thus parameters representing the retention curves for spodic horizons and eluvial horizon below the top-soil were estimated using the soil texture and the bulk density information with pedotransfer function implemented in Rosetta code (Schaap et al., 2001).

The estimated soil hydraulic parameters (SHP) for the lower horizons below the top soil are depicted in

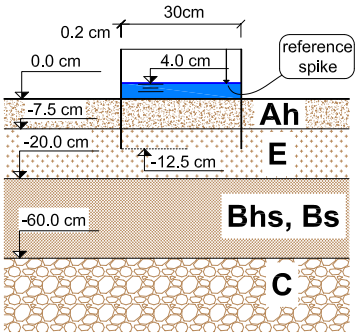

Figure 1: Scheme of the single ring infiltration experiment and the soil layers.

table 1.

Table 1: Soil hydraulic parameters for the lower horizons.

Ranges of depths, horizon(s)	SHPs				
[cm]	θ_s [-]	α [m^{-1}]	n [-]	K_s [ms^{-1}]	S_s [m^{-1}]
7.5 - 20, eluvial E	0.46	4.65	1.7408	4.4×10^{-6}	0
20 - 60 spodic Bhs and Bs	0.47	2.21	1.4494	1.5×10^{-6}	0
$>$ 60 weathered bedrock C	0.50	3.52	4.03	8.5×10^{-6}	0

2.1.4. Obtaining unsteady infiltration data for the top soil inverse modeling

The purpose of this section is to explain the methodology used for obtaining the data for the proposed inverse analyses.

For the O+Ah horizon, the smoothed experimental data for unsteady single ring (SR) infiltration were used as the input for inverse modeling of the Richards equation, where the entire parameter set, as given in section 2.1.2, was identified. In brief, the experimental setup was as follows. A steel ring 30 cm in inner diameter, 25 cm in length, and 2 mm in thickness was inserted into the soil to a depth of 12.5 cm, see figure 1. The depth of ponding was kept approximately at a constant level defined by a reference spike, which was placed 4 cm above the surface of the soil. An average experiment duration was 60 minutes.

A total of 22 SR experiments were conducted on the site. Statistical description of these infiltration data is given by (Jačka et al., 2016), see datasets collected on site 3. The experiments were evaluated as follows. In order to eliminate noise from the experimental values, each SR experiment data set was smoothed. It was observed that the Schwarzendruber analytical model of one-dimensional infiltration exhibited an excellent

fitting quality, with the mean Nash-Sutcliffe model efficiency coefficient value estimated as 0.9974. Thus we made use of exponential data smoothing here. The Schwarzendruber equation for cumulative infiltration states that

$$I(t) = \frac{c_0 \left(1 - \exp\left(-c_1\sqrt{t}\right)\right)}{c_1} + c_2 t, \tag{1}$$

where I is the cumulative infiltration $[L]$, and where the parameter set $c_{0,1,2}$, is usually expressed in terms of SHPs. This physically based interpretation of the Schwarzendruber parameters is disregarded here, because our infiltration model does not meet the prerequisites for the Schwarzendruber model. The Schwarzendruber model was considered here as some exponential smoothing function only without any physically based interpretation.

According to the normality tests, all three datasets of $c_{0,1,2}$ parameters can be well approximated using a log-normal distribution. The geometric mean is therefore suitable for estimating representative values of these parameters. Representative values are as follows: $c_0 = 8.55 \times 10^{-4}$ m.s$^{-0.5}$, $c_1 = 0.1132$ [-], and $c_2 = 5.16 \times 10^{-6}$ m.s^{-1}. The evaluated representative parameter set, together with model (1), will be used here as an input curve for identifying the top soil hydraulic parameters (SHP). SHPs of the lower horizons were estimated from direct measurements, as will be described in the next section.

It is already apparent at this moment, that if the infiltration experiment can be so well approximated by the three parametric model (1), then the five parametric SHPs representation potentially leads to over-parametrization and makes the model non-identifiable, which is already a well known issue, see e.g. (Bellman and Åström, 1970).

2.2. Inverse modeling procedures

2.3. Mathematical model of the field infiltration experiment – governing equation

The field infiltration experiment is characterized by variably saturated conditions ranging between unsaturated and saturated states. The geometry of the flow is inherently three-dimensional, but the domain dimension can be reduced by considering the axisymmetric geometry. It is well known that the flux in porous media under variably saturated conditions can be expressed by the Darcy-Buckingham law (Buckingham, 1907)

$$\mathbf{q} = -\mathbf{K}(\theta)\nabla H, \tag{2}$$

where $\mathbf{q}$ is the volumetric flux $[L.T^{-1}]$, H is the total hydraulic head $[L]$ defined as $H = h + z$, where h is the pressure head $[L]$, z is the potential head $[L]$, θ is the water content [-], and $\mathbf{K}(\theta)$ is the unsaturated

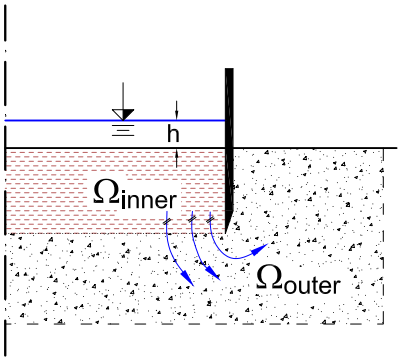

Figure 2: Scheme of the flow domain and the streamlines of infiltration experiment.

hydraulic conductivity $[L.T^{-1}]$; in general it is a second order tensor. The relation $\theta(h)$ is referred to as the retention curve, see e.g. (van Genuchten, 1980).

The law of mass conservation for incompressible flow in cylindric coordinates is expressed as (see e.g. (Bear, 1979))

$$-\frac{\partial V}{\partial t} = \frac{\partial q_r}{\partial r} + \frac{q_r}{r} + \frac{\partial q_\alpha}{\partial \alpha} + \frac{\partial q_z}{\partial z}, \tag{3}$$

where V is the volume function [-], r is the radial coordinate, α is the angular coordinate, z is the vertical coordinate, and $q_{r,\alpha,z}$ is the volume flux $[L.T^{-1}]$. The ring infiltration experiment is characterized by rotational symmetric flow, so the angular derivative vanishes. Then the governing equation for variably saturated and rotational symmetric flow is obtained by substituting the flux in (3) by the Darcy-Buckingham law (2). Together with the consideration of linear elasticity for a porous medium the variably saturated axisymmetric flow in isotropic media is governed by

$$\left(\frac{\mathrm{d}\theta}{\mathrm{d}h} + S_s\frac{\theta(h)}{\theta_s}\right)\frac{\partial h}{\partial t} = \frac{\partial K(h)\frac{\partial H}{\partial z}}{\partial z} + \frac{\partial K(h)\frac{\partial H}{\partial r}}{\partial r} + c(\mathbf{x})\frac{\partial H}{\partial r}, \tag{4}$$

where S_s is the specific storage $[L^{-1}]$, θ_s is the saturated water content [-], $c(\mathbf{x})$ is the coefficient of the convection for r coordinate $[T^{-1}]$, which has to be further explained, and the vector x is a vector of the spatial coordinates $\mathbf{x} = \binom{r}{z}$.

Let us consider the model of the infiltration experiment depicted in figure 2. Let the entire flow domain $\Omega = \Omega_{inner} \cup \Omega_{outer}$, where Ω_{outer} is the flow domain outside the infiltration ring and Ω_{inner} is the flow domain within the infiltration ring, exactly as depicted in figure 3. It is apparent that the streamlines inside subdomain Ω_{inner} are parallel, but the streamlines outside the infiltration ring (inside Ω_{outer}) are

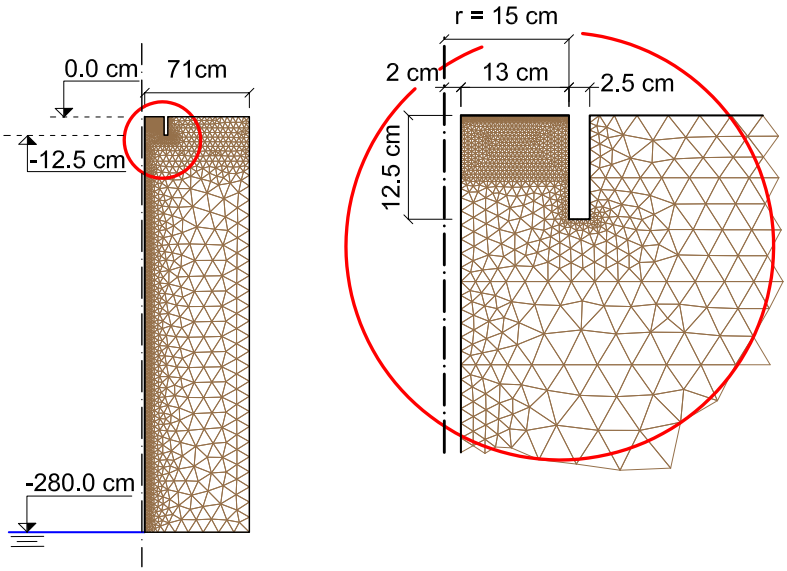

Figure 3: Scheme of the computational domain geometry and domain triangularization.

only axisymmetric. Then the convection coefficient $c(\mathbf{x})$ is defined as follows

$$c(\mathbf{x}) = \begin{cases} 0, & \forall \mathbf{x} \in \Omega_{inner} \\ \frac{1}{r}K(h), & \forall \mathbf{x} \in \Omega_{outer}. \end{cases} \tag{5}$$

Note that the flow boundary should not be identical with the axis of rotation symmetry ($r > 0$). Moreover, using the standard finite element method approximation, r should even be sufficiently greater than zero (depending on your mesh discretization) to prevent convective dominance (details explained in section 2.3.1). The constitutive relation $\theta(h)$ was substituted by the van Genuchten law (van Genuchten, 1980), and the constitutive relation $K(h)$ was supplied by the Mualem law (Mualem, 1976).

2.3.1. Domain scheme, initial conditions and boundary conditions

The goal of the model was to achieve cumulative infiltration – the cumulative flux over the top Dirichlet boundary. The computational domain is depicted in figure 3 together with the discretization mesh. The location of the top boundary was natural – it is the ground surface (inside the ring, it is the Dirichlet condition defining the ponding depth; outside the infiltration ring it is the Neumann condition – the no-flow boundary). But locating the bottom boundary was more problematic. The following options are available

- the no-flow boundary (Neumann)

- the free drainage boundary (Neumann)
- the groundwater level - zero pressure head (Dirichlet)

It is apparent that the wetting front originating from our infiltration experiment affects the soil column only to a certain depth. Defining the Neumann no-flow boundary at a sufficient depth would therefore probably not have a significant effect on the derivative of the solution of (4) at the top boundary. At the same time, the no-flow boundary is physically incorrect, so this option was rejected. The second option – the free drainage boundary – would be completely incorrect here. The free drainage boundary defines fluxes that probably do not appear in our system at all. Above all, if we consider here the initial condition as a hydrostatic state, and so

$$\frac{\partial h}{\partial z}(x) = -1, \quad \forall x \in \Omega. \tag{6}$$

The free drainage boundary condition, which is defined as

$$\frac{\partial h}{\partial \mathbf{n}}(x) = 0, \quad \forall (x,t) \in \Gamma_{\text{free drainage}} \times [0,T). \tag{7}$$

is in a conflict with the initial condition (since the outer normal vector $\mathbf{n} = \left(\begin{smallmatrix} 0 \\ 1 \end{smallmatrix}\right)$), which is again physically incorrect, and produces further computational costs. The reason for the extra computational costs is that the nonlinear equation solver (in this case Picard method) together with the iterative linear equation solver (in this case preconditioned conjugate gradient method) treats iteration increments for the bottom boundary, which is in an ideal case out of the reach of the infiltration experiment, and naturaly there is no physical process taking place in the initial time levels. The computational process, that is produced on the bottom boundary in the initial time levels with such boundary setup, originates from the initial and boundary condition mismatch.

It turns out that the only physically correct boundary condition for the bottom boundary is the Dirichlet boundary, which represents the groundwater table. The average depth of the groundwater table was known, it is approximately -280 cm below the surface. However, with this particular setup the domain became extremely narrow and deep. However, since the solution at greater depths is not crucial for estimating the cumulative infiltration we can use coarser discretization there. Further, if we apply the adaptive domain decomposition algorithm (*dd*-adaptivity), see (Kuraz et al., 2013a, 2014, 2015), the non-active parts of the computational domain are sequentially activated and deactivated, and then our current domain extension does not have a significant effect on the computational speed, but our domain description is consistent with

the real physical porous medium system.

Another issue is the left hand side domain boundary, which should be located at a sufficient distance from the axis of anisotropy, because of the term $\frac{1}{r}$ in (5). The Peclet number representing the numerical stability of convection-diffusion problems (see e.g. (Knobloch, 2008)) is in our case given as follows

$$Pe = \frac{\frac{\partial h}{\partial r}\Delta x}{2r}, \tag{8}$$

where Δx is the discretization length $[L]$. Since our mesh is triangular, Δx can be roughly assumed to be the greatest triangle altitude (since we assume some mesh quality properties). Then a sufficient distance from the axis of anisotropy is such that the Peclet number is sufficiently low. If we want to make our computation free of spurious oscillations, a sufficiently low Peclet number means $Pe \leq 1$. Therefore, the distance from the axis of anisotropy is given by the domain discretization step at the left hand side boundary. The selected discretization step at the left hand side boundary was assumed as $\Delta x = 2$ cm. The domain was therefore detached by 2 cm from the axis of anisotropy (assuming that $\frac{\partial h}{\partial r}(r,z) < 1,\ \forall (r,z) \in \Omega_{outer}$).

In order to avoid the non-Lipschitz boundary (or any boundary with a shape that is close to the non-Lipschitz boundary) the infiltration ring thickness was oversized for 2.5 cm. It is obvious that the real ring thickness is much smaller (in our case 2 mm), but using the real ring thickness yields possible numerical issues, since then the domain has the appearance of a textbook case of a non-Lipschitz bounded domain, see e.g. (??, ??). However, it is also expected, that oversizing the ring thickness does not significantly affect the solution at the top Dirichlet boundary.

I will add some reference here

The right hand side boundary was located at a distance $r = 73$ cm, it means 50 cm from the infiltration ring.

The locations of the domain boundaries are depicted in figure 4. The boundary conditions are specified as follows

$$\begin{aligned} &h(x,t) = 4 \text{ cm} \Rightarrow H(x,t) = 4 \text{ cm}; \quad \forall (x,t) \in \Gamma_1 \times [0,T), \\ &\frac{\partial H}{\partial \mathbf{n}} = 0; \quad \forall (x,t) \in \Gamma_2 \times [0,T), \\ &h(x,t) = 0 \text{ cm} \ \Rightarrow \ H(x,t) = -280.0 \text{ cm}; \quad \forall (x,t) \in \Gamma_3 \times [0,T). \end{aligned} \tag{9}$$

where T is the simulation end time $[T]$, and $\mathbf{n}$ is the boundary normal vector.

The initial condition was assumed as a steady state solution of (4) with the boundary $\Gamma_1 \cup \Gamma_2$ assumed as a no-flow boundary – thus the entire domain Ω was considered in a hydrostatic state. Then the initial

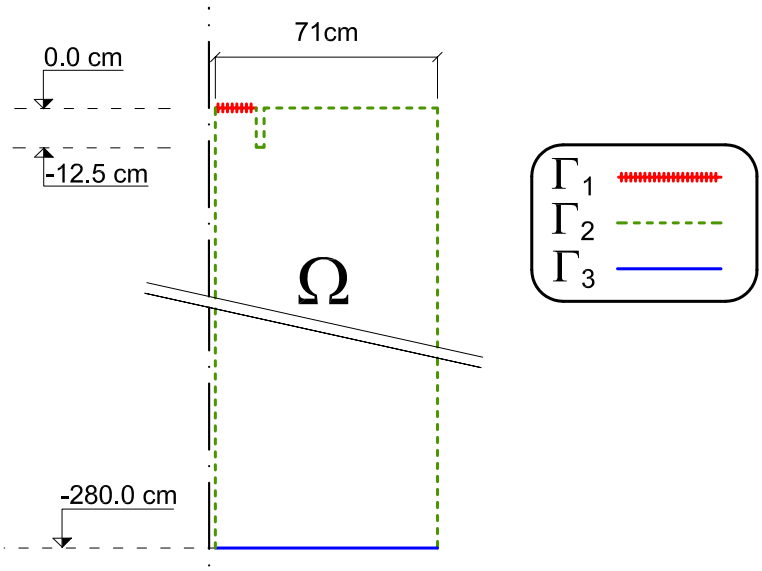

Figure 4: Scheme of the computational domain geometry and the domain boundaries.

condition states that

$$H(x) = -280.0 \text{ cm}; \quad \forall x \in \Omega, \tag{10}$$

and thus $\frac{\partial h}{\partial z} = -1$.

2.3.2. Numerical solution, temporal and spatial discretization, automatic calibration methodology

Equation (4) was implemented into DRUtES library (Kuraz and Mayer, 2008). This is an object-oriented library written in Fortran 2003/2008 standard for solving nonlinear coupled convection-diffusion-reaction type problems. The problem was approximated by the linear finite element method for spatial derivatives and Rothe's method for temporal derivatives. The nonlinear operator was treated with the Schwarz-Picard method – an adaptive domain decomposition (*dd*-adaptivity) – with the ability to activate and deactivate subregions of the computational domain sequentially, see works (Kuraz et al., 2013a, 2014, 2015)).

The domain was nonuniformly discretized by a triangular mesh. The smallest spatial step was considered for the top layers inside the infiltration ring, close to the Dirichlet boundary. The mesh is depicted on figure 3. The minimal spatial step was 0.5 cm, and the maximal spatial step was 20 cm. The domain was discretized with 2097 nodes and 3861 elements. The coarse mesh for the *dd*-adaptivity method was a uniform quadrilateral mesh with elements 17.75×28.0 cm, i.e. a total of 40 coarse elements and 55 nodes. The purpose of the coarse mesh is to organize the elements of the domain triangularization into so-called clusters, which form a basic unit for the adaptive domain decomposition used here for solving the nonlinear

problem, details can be found in (Kuraz et al., 2015).

The spatial and temporal discretization of (4) leads into sequential solutions of systems of non-linear equations, see e.g. (Kuraz et al., 2013a). The system was linearized as discussed in (Kuraz and Mayer, 2013; Kuraz et al., 2013b), and so the numerical solution requires an iterative solution of

$$\mathbf{A}(\mathbf{x}_l^k)\mathbf{x}_l^{k+1} = \mathbf{b}(\mathbf{x}_l^k), \tag{11}$$

where k denotes the iteration level, and l denotes the time level, until

$$||\mathbf{x}_l^{k+1} - \mathbf{x}_l^k||_2 < \varepsilon, \tag{12}$$

where ε is the desired iteration criterion. The iterations required for (11) to converge are denoted as the outer iterations. It is apparent that the number of the required outer iterations depends on the required value of ε criterion.

The method (11) degenerates into a kind of semiexplicit approximation if the error criterion ε was taken from the extended real numbers, $\varepsilon \in \overline{\mathbb{R}}$, and assigned as $\varepsilon = +\infty$. This semiexplicit approximation is denoted as

$$\mathbf{A}(\mathbf{x}_{l-1})\mathbf{x}_l = \mathbf{b}(\mathbf{x}_{l-1}). \tag{13}$$

This semiexplicit method always requires just a single outer iteration. It is apparent that for short time stepping the method converges to the exact solution. But for the inappropriate time stepping, the method diverge from the exact solution faster than the method (11). However, the method (13) is still free of possible issues related to the convergence of the nonlinear operator.

Since the infiltration flux is obtained from the numerical derivative of the solution of (4), and since it is well known that inaccurate approximation of the capacity term (time derivative term) yields inaccurate mass properties (Celia et al., 1990), we are aware of a possible impact of spatial and temporal discretization on the identified SHP values. But we are also aware of possible difficulties with convergence of the linearized discrete system (11) for certain combinations of SHPs values within the ranges given in table 2 during the automatic calibration, as discussed in Binley and Beven (2003). And thus the following methodology for the automatic calibration was proposed here.

(**i**) Proceed the calibration procedure with the quasi-explicit stable numerical technique for treating the

Check if this is understandable

nonlinear operator explained in equation (13), with the initial time step $t_{init} = 10^{-6}$ hrs, and for each subsequent time level l, $\Delta t_l = 1.05\Delta t_{l-1}$, where $l = \{1, n_t\}$, where n_t is the number of time levels used for the temporal discretization. The ranges of parameters for this calibration are given in table 2, so the maximal values of SHP are defined as a vector $\mathbf{p}^{r_f}_{max}$, and the minimal values are defined as a vector $\mathbf{p}^{r_f}_{min}$. The spatial discretization for this step of calibration was given in the beginning of this section – 2097 nodes and 3861 elements. Let us assume that this discretization is given by a mesh density function $\Delta(\mathbf{x})^{r_f}$. The function $\Delta(\mathbf{x})^{r_f}$ is understood as a spatial distribution of mesh size density, which was used as an input for the mesh generator T3D (Rypl, Daniel, 2004). The superscript r_f defines the refinement level, where $r_f = 0$ at this particular stage, and the vector $\mathbf{x}$ refers to spatial coordinates inside the domain Ω.

(**ii**) Let us pressume that this inverse model will have more than just a single solution, this is an assumption of multimodality, which is based on (Binley and Beven, 2003).

- Then this calibration will generate vectors of SHPs values $\mathbf{p}^{i_e}_{r_f}$, where the superscript $i_e = \{1, ..., n_e\}$, where n_e denotes the number of local extremes.

(**iii**) To validate the inverse modeling results, select physically acceptable local extremes with good fitting qualities, and create a scatter plot of the objective function in the local extreme neighborhood with improved temporal integration and spatial discretization. The improvement of the numerical treatment will be processed as follows:

Increase the discretization level

$$r_f = r_f + 1, \tag{14}$$

and update the following parameters of the numerical treatment

$$\begin{aligned} \Delta(\mathbf{x})^{r_f} &= \frac{\Delta(\mathbf{x})^{r_f-1}}{2}, \\ \varepsilon^{r_f} &= 10^{-3} \text{ cm} \quad \text{if } r_f = 0, \text{ else } \quad \varepsilon^{r_f} = \frac{\varepsilon^{r_f-1}}{10}, \\ t^{r_f}_{init} &= \frac{t^{r_f-1}_{init}}{10} \text{ hrs.} \end{aligned} \tag{15}$$

If $r_f > 0$, then the nonlinear problem represented now by (11) will be solved by the Schwarz-Picard method – an adaptive domain decomposition (Kuraz et al., 2015). To validate the inverse model solution for $r_f - 1$ discretization level perform the following:

(a) Compare the scatter plots for the selected local extreme i_e created with discretization r_f and $r_f - 1$. For this local extreme a vector of SHP parameters $\mathbf{p}^{i_e}_{r_f-1}$ is handled.

(b) **If** the scatter plots differ significantly

- Proceed the calibration again with the new parameter range defined as $\mathbf{p}_{max} = 1.1\mathbf{p}^{i_e}_{r_f-1}$ and $\mathbf{p}_{min} = 0.9\mathbf{p}^{i_e}_{r_f-1}$. This new calibration will update the vector $\mathbf{p}^{i_e}_{r_f-1}$ to $\mathbf{p}^{i_e}_{r_f}$.
- Increase the discretization level r_f as $r_f = r_f + 1$, perform the update (15), return to (**iii**)a, and check the condition (**iii**)b.

(c) **else**

- Exit the calibration process.

(**iv**) At this step the vectors of the validated inverse model solutions $\mathbf{p}^{i_e}$ (SHP parameter sets) are available for discussion.

In the second stage the unknown SHPs parameters will be reduced and the automatic calibration using the initial mesh together with the simple quasi-explicit approximation (13) will proceed. The unknown SHPs parameters will be sequentially reduced in the following order until just a single extreme will be identified.

(**I**) S_s – specific storage is often neglected for the unsaturated zone, and thus for the first unknown parameter reduction will be assigned $S_s = 0$ m^{-1}

(**II**) θ_s – water content is often easy to measure directly, despite there are no available data for top soil layer, let's presume $\theta_s = 0.6$.

(**III**) K_s – if the identifiability of the inverse model will require also reduction of K_s, then this inverse task became inappropriate for any further analyses, and the conducted SR measurements will be declared as non-identifiable setup for SHP parameters.

The following sections will further explain the definition of the objective function and the parameter identification algorithm.

2.4. Parameter identification, a definition of the objective function

The soil hydraulic parameters (SHP) of the top soil that will be identified were specified in section 2.1.2. Since the parameters will be identified using a stochastic method, we have to introduce a physically reasonable range for each parameter. The ranges for the SHPs are specified in table 2.

Table 2: Ranges of SHPs ($\mathbf{p}_{max}$ and $\mathbf{p}_{min}$) for identifying the SHPs in the top-soil layer for *refinement level* $r_f = 0$.

θ_s [-]	α [m^{-1}]	n [-]	K_s [$\mathrm{m.s}^{-1}$]	S_s [$\mathrm{m}^{-}1$]
0.25 – 0.90	0.01 – 5.0	1.05 – 2.10	10^{-7} – 10^{-4}	0.0 – 10.0

The objective function is defined in the following paragraph.

Let $\bar{I}(\mathbf{p}, t)$ be the cumulative infiltration obtained from solving the mathematical model (4) bounded by the initial and boundary conditions defined in section 2.3.1 for a certain vector of SHPs parameters $\mathbf{p}$ considered as

$$\bar{I}(\mathbf{p}, t) = \frac{\int_0^t \int_{\Gamma_1} -K \frac{\partial H}{\partial \mathbf{n}}(t) \mathrm{d}\Gamma_1 \mathrm{d}t}{\int_{\Gamma_1} \mathrm{d}\Gamma_1}. \tag{16}$$

Let $I(t)$ be the cumulative infiltration defined by (1) with parameters given in section 2.1.4. Then the objective function was defined for three different criteria in order to avoid ill-posed objective function definition.

The objective functions were defined as follows:

I. First criterion Ψ_1 was defined as L_2 norm of the difference between the experimental and model data and thus

$$\Psi_1(\mathbf{p}) = \sqrt{\int_0^{T_{end}} \left(\bar{I}(\mathbf{p}, t) - I(t)\right)^2 \mathrm{d}t}, \tag{17}$$

where T_{end} is the final simulation time $[T]$, which is indeed the root mean square error for continous functions. This could be understood as a global criterion.

II. Second criterion was the L_∞ norm of the difference between the experimental and model data and thus

$$\Psi_2(\mathbf{p}) = \sup\left(\sqrt{\left(\bar{I}(\mathbf{p}, t) - I(t)\right)^2}\right), \quad t \in (0, T_{end}). \tag{18}$$

This could be understood as a local criterion.

III. Third criterion was considered as the difference between the final derivatives between the model data and the experimental data

$$\Psi_3(\mathbf{p}) = \sqrt{\left(\frac{\mathrm{d}\bar{I}(\mathbf{p}, T_{end})}{\mathrm{d}t} - \frac{\mathrm{d}I(T_{end})}{\mathrm{d}t}\right)^2}. \tag{19}$$

This could also be again understood as a local criterion.

And so we have applied here a multi-objective optimization. However, it is apparent that minimizing the objective function (17) also minimizes the objective functions (18) and (19). The aim of this multi-objective definition was improving the conditioning of this inverse problem. If we considered the objective function (17) only, then we were probably able to obtain the same solution as with this multi-objective definition with slower convergence of optimization procedure only (the selection of the optimization algorithm will be explained in the following section 2.4.1). This multi-objective function definition is based on experience from our previous attempts in inverse analyses of this infiltration problem.

2.4.1. Optimization method

The most traditional way of dealing of multiple objectives in optimization is the Weighted Sum Method (WSF). Each objective out of kk objectives $f_i(\mathbf{x})$ is multiplied by user defined weights w_i and their sum is optimized. The problem is converted into single criteria optimization:

$$F(\mathbf{x}) = \sum_{i=1}^{kk} w_i f_i(\mathbf{x}), \qquad \sum_{i=1}^{kk} w_i = 1, \quad w_i \geq 0, \tag{20}$$

and any single-objective optimization method can be used to solve (20). Although this method is really easy and intuitive, the biggest obstacle is in setting the weights. The weights express the relative importance of individual objectives, which, in real world applications, is difficult to determine. The success of the WSM depends also on scaling of objectives; all of them should have more or less the same order of magnitude to affect the value of $F(\mathbf{x})$ similarly. Therefore, not only weight vector must be set, but also a normalization of objectives must be performed. Similarly to weight vector, it is difficult to determine in advance which objectives' values can be reached and accordingly, to properly set the normalization vector.

It seems to be advantageous to use population-based Evolutionary Algorithms to obtain the Pareto set for general multi-objective optimization problem.

In this contribution, a genetic algorithm called GRADE (Ibrahimbegović et al., 2004; Kucerova, 2007) was applied. It is a real-coded genetic algorithm combining the ideas of genetic operators: cross-over, mutation and selection taken from the standard genetic algorithm and the idea of differential operator taken from the differential evolution. Moreover, the algorithm GRADE is supported with the niching method CERAF, which was developed based on an idea of enhancing the algorithm with memory and restarts (Hrstka and Kucerova, 2004). When the GRADE algorithm loses the convergence, the current position of the optimization algorithm is marked as a local extreme and a forbidden area is build around in order to forbid the optimization

algorithm again to fall into the same local extreme. Hence all inspected local extremes are stored in memory and can be inspected after the optimization.

The main setting of the optimization procedure was as follows: the population of the genetic algorithm contains 30 independent solutions, the whole identification stops after 20.000 objective function evaluations and a local extreme was marker after 600 evaluations without any improvement.

3. Results and discussion

4. Conclusions

5. Acknowledgement

Financial support from the Czech Science Foundation (research project GACR 13-11977P) is gratefully acknowledged.

??, ?? ?? ??

Angulo-Jaramillo, R., Vandervaere, J.P., Roulier, S., Thony, J.L., Gaudet, J.P., Vauclin, M., 2000. Field measurement of soil surface hydraulic properties by disc and ring infiltrometers: A review and recent developments. Soil Tillage Res. 55, 1–29. doi:10.1016/S0167-1987(00)00098-2.

Bagarello, V., Prima, S.D., Iovino, M., 2017. Estimating saturated soil hydraulic conductivity by the near steady-state phase of a beerkan infiltration test. Geoderma 303, 70 – 77. URL: http://www.sciencedirect.com/science/article/pii/S001670611730201X, doi:https://doi.org/10.1016/j.geoderma.2017.04.030.

Bear, J., 1979. Hydraulics of groundwater. McGraw-Hill series in water resources and environmental engineering, McGraw-Hill International Book Co.

Bellman, R., Åström, K., 1970. On structural identifiability. Mathematical Biosciences 7, 329 – 339. URL: http://www.sciencedirect.com/science/article/pii/002555647090132X, doi:https://doi.org/10.1016/0025-5564(70)90132-X.

Binley, A., Beven, K., 2003. Vadose zone flow model uncertainty as conditioned on geophysical data. Ground Water 41, 119–127. URL: http://dx.doi.org/10.1111/j.1745-6584.2003.tb02576.x, doi:10.1111/j.1745-6584.2003.tb02576.x.

Buckingham, E., 1907. Studies on the movement of soil moisture. USDA Bureau of Soils – Bulletin 38.

Celia, M.A., Bouloutas, E.T., Zarba, R.L., 1990. A general mass-conservative numerical solution for the unsaturated flow equation. Water Resources Research 26, 1483–1496. doi:10.1029/WR026i007p01483.

Cheng, Q., Chen, X., Chen, X., Zhang, Z., Ling, M., 2011. Water infiltration underneath single-ring permeameters and hydraulic conductivity determination. J. Hydrol. 398, 135–143. doi:10.1016/j.jhydrol.2010.12.017.

Fodor, N., Sándor, R., Orfánus, T., Lichner, L., Rajkai, K., 2011. Evaluation method dependency of measured saturated hydraulic conductivity. Geoderma 165, 60–68. doi:10.1016/j.geoderma.2011.07.004.

van Genuchten, M., 1980. Closed-form equation for predicting the hydraulic conductivity of unsaturated soils. Soil Science Society of America Journal 44, 892–898. URL: http://www.scopus.com/inward/record.url?eid=2-s2.0-0019057216&partnerID=40&md5=1a9a45e1c2b571c00ebb9a9f9ebaaf92.

Hrstka, O., Kucerova, A., 2004. Improvements of real coded genetic algorithms based on differential operators preventing premature convergence. Advances in Engineering Software 35, 237 – 246. doi:http://dx.doi.org/10.1016/S0965-9978(03)00113-3.

Hwang, S.I., Powers, S.E., 2003. Estimating unique soil hydraulic parameters for sandy media from multi-step outflow experiments. Advances in Water Resources 26, 445 – 456. URL: http://www.sciencedirect.com/science/article/pii/S0309170802001070, doi:https://doi.org/10.1016/S0309-1708(02)00107-0.

Ibrahimbegović, A., Knopf-Lenoir, C., Kucerova, A., Villon, P., 2004. Optimal design and optimal control of structures undergoing finite rotations and elastic deformations. International Journal for Numerical Methods in Engineering 61, 2428–2460.

Inoue, M., Šimøunek, J., Shiozawa, S., Hopmans, J., 2000. Simultaneous estimation of soil hydraulic and solute transport parameters from transient infiltration experiments. Advances in Water Resources 23, 677 – 688. URL: http://www.sciencedirect.com/science/article/pii/S0309170800000117, doi:https://doi.org/10.1016/S0309-1708(00)00011-7.

Jačka, L., Pavlásek, J., Jindrová, M., Bašta, P., Černý, M., Balvín, A., Pech, P., 2012. Steady infiltration rates estimated for a mountain forest catchment based on the distribution of plant species. J. For. Sci. 58, 536–544.

Jačka, L., Pavlásek, J., Kuráž, V., Pech, P., 2014. A comparison of three measuring methods for estimating the saturated hydraulic conductivity in the shallow subsurface layer of mountain podzols. Geoderma 219–220, 82 – 88. doi:10.1016/j.geoderma.2013.12.027.

Jačka, L., Pavlásek, J., Pech, P., Kuráž, V., 2016. Assessment of evaluation methods using infiltration data measured in heterogeneous mountain soils. Geoderma 276, 74 – 83. URL: http://www.sciencedirect.com/science/article/pii/S0016706116301823, doi:http://dx.doi.org/10.1016/j.geoderma.2016.04.023.

Knobloch, P., 2008. On the choice of the supg parameter at outflow boundary layers. Advances in Computational Mathematics 31, 369. URL: https://doi.org/10.1007/s10444-008-9075-6, doi:10.1007/s10444-008-9075-6.

Kohne, J., Mohanty, B., Simunek, J., 2006. Inverse dual-permeability modeling of preferential water flow in a soil column and implications for field-scale solute transport. Vadose zone journal 5, 59 – 76. doi:http://dx.doi.org/10.2136/vzj2005.0008.

Kool, J., Parker, J., Van Genuchten, M., 1985. Determining soil hydraulic properties from one-step outflow experiments by parameter estimation. i. theory and numerical studies. Soil Science Society of America 49, 1348 – 1354.

Kucerova, A., 2007. Identification of nonlinear mechanical model parameters based on softcomputing methods. Ph.D. thesis. Ecole Normale Supérieure de Cachan, Laboratoire de Mécanique et Technologie.

Kuraz, M., Mayer, P., 2008. Drutes – an opensource library for solving coupled nonlinear convection-diffusion-reaction equations. URL: http://www.drutes.org.

Kuraz, M., Mayer, P., 2013. Algorithms for solving darcian flow in structured porous media. Acta Polytecnica 53, 347–358.

Kuraz, M., Mayer, P., Havlicek, V., Pech, P., 2013a. Domain decomposition adaptivity for the richards equation model. Computing 95, 501–519. URL: http://dx.doi.org/10.1007/s00607-012-0279-8, doi:10.1007/s00607-012-0279-8.

Kuraz, M., Mayer, P., Havlicek, V., Pech, P., Pavlasek, J., 2013b. Dual permeability variably saturated flow and contaminant transport modeling of a nuclear waste repository with capillary barrier protection.

Applied Mathematics and Computation 219, 7127 – 7138. doi:http://dx.doi.org/10.1016/j.amc.2011.08.109.

Kuraz, M., Mayer, P., Pech, P., 2014. Solving the nonlinear richards equation model with adaptive domain decomposition. Journal of Computational and Applied Mathematics 270, 2 – 11. URL: http://www.sciencedirect.com/science/article/pii/S0377042714001502, doi:http://dx.doi.org/10.1016/j.cam.2014.03.010. fourth International Conference on Finite Element Methods in Engineering and Sciences (FEMTEC 2013).

Kuraz, M., Mayer, P., Pech, P., 2015. Solving the nonlinear and nonstationary richards equation with two-level adaptive domain decomposition (dd-adaptivity). Applied Mathematics and Computation 267, 207 – 222.

Lassabatère, L., Angulo-Jaramillo, R., Soria Ugalde, J.M., Cuenca, R., Braud, I., Haverkamp, R., 2006. Beerkan estimation of soil transfer parameters through infiltration experiments–best. Soil Science Society of America Journal 70, 521 – 532. doi:http://dx.doi.org/10.2136/sssaj2005.0026.

Mous, S., 1993. Identification of the movement of water in unsaturated soils: the problem of identifiability of the model. Journal of Hydrology 143, 153 – 167. URL: http://www.sciencedirect.com/science/article/pii/002216949390093O, doi:https://doi.org/10.1016/0022-1694(93)90093-O. xVI General Assembly of the European Geophysical Society.

Mualem, Y., 1976. A new model for predicting the hydraulic conductivity of unsaturated porous media. Water Resources Research 12, 513–522. URL: http://www.scopus.com/inward/record.url?eid=2-s2.0-0016961814&partnerID=40&md5=67a0ce14b8c2f2d218312a09532e171a, doi:10.1029/WR012i003p00513. cited By 2855.

Ramos, T., Goncalves, M., Martins, J., van Genuchten, M., Pires, F., 2006. Estimation of soil hydraulic properties from numerical inversion of tension disk infiltrometer data. VADOSE ZONE JOURNAL 5, 684–696. doi:10.2136/vzj2005.0076.

Reynolds, W.D., 2008a. Saturated hydraulic properties: Ring infiltrometer, in: Carter M.R., Gregorich, E.G. [Eds.], Soil Sampling and Methods of Analysis, 2nd ed. CRC Press Taylor & Francis, Boca Raton, USA, pp. 1043–1056.

Reynolds, W.D., 2008b. Saturated hydraulic properties: Well permeameter, in: Carter M.R., Gregorich, E.G. [Eds.], Soil Sampling and Methods of Analysis, 2nd ed. CRC Press Taylor & Francis, Boca Raton, USA, pp. 1025–1042.

Rezaei, M., Seuntjens, P., Shahidi, R., Joris, I., Boënne, W., Al-Barri, B., Cornelis, W., 2016. The relevance of in-situ and laboratory characterization of sandy soil hydraulic properties for soil water simulations. Journal of Hydrology 534, 251 – 265. URL: http://www.sciencedirect.com/science/article/pii/S0022169416000044, doi:http://dx.doi.org/10.1016/j.jhydrol.2015.12.062.

Richards, L.A., 1931. Capillary conduction of liquids through porous mediums. Journal of Applied Physics 1, 318–333. doi:10.1063/1.1745010.

Rypl, Daniel, 2004. T3D Mesh Generator. Department of Mechanics, CTU in Prague, Czech Republic. Prague, Czech Republic. URL: http://mech.fsv.cvut.cz/~dr/t3d.html.

Schaap, M.G., Leij, F.J., van Genuchten, M.T., 2001. rosetta: a computer program for estimating soil hydraulic parameters with hierarchical pedotransfer functions. J. Hydrol. 251, 163 – 176. doi:http://dx.doi.org/10.1016/S0022-1694(01)00466-8.

Scharnagl, B., Vrugt, J.A., Vereecken, H., Herbst, M., 2011. Inverse modelling of in situ soil water dynamics: investigating the effect of different prior distributions of the soil hydraulic parameters. Hydrology and Earth System Sciences 15, 3043–3059. URL: http://www.hydrol-earth-syst-sci.net/15/3043/2011/, doi:10.5194/hess-15-3043-2011.

Schwartz, R., Evett, S., 2002. Estimating hydraulic properties of a fine-textured soil using a disc infiltrometer. SOIL SCIENCE SOCIETY OF AMERICA JOURNAL 66, 1409–1423.

Simunek, J., van Genuchten, M., T., Gribb, M., Hopmans, J.W., 1998. Parameter estimation of unsaturated soil hydraulic properties from transient flow processes1. Soil Tillage Res. 47, 27 – 36. doi:http://dx.doi.org/10.1016/S0167-1987(98)00069-5.

Simunek, J., Wendroth, O., van Genuchten, M., 1999. Estimating unsaturated soil hydraulic properties from laboratory tension disc infiltrometer experiments. WATER RESOURCES RESEARCH 35, 2965–2979. doi:{10.1029/1999WR900179}.

Ventrella, D., Losavio, N., Vonella, A., Leij, F., 2005. Estimating hydraulic conductivity of a fine-textured

soil using tension infiltrometry. Geoderma 124, 267 – 277. doi:http://dx.doi.org/10.1016/j.geoderma.2004.05.005.

Verbist, K., Cornelis, W.M., Gabriels, D., Alaerts, K., Soto, G., 2009. Using an inverse modelling approach to evaluate the water retention in a simple water harvesting technique. HYDROLOGY AND EARTH SYSTEM SCIENCES 13, 1979–1992.

Xu, X., Lewis, C., Liu, W., Albertson, J., Kiely, G., 2012. Analysis of single-ring infiltrometer data for soil hydraulic properties estimation: Comparison of best and wu methods. Agricultural Water Management 107, 34 – 41. URL: http://www.sciencedirect.com/science/article/pii/S0378377412000200, doi:https://doi.org/10.1016/j.agwat.2012.01.004.

Younes, A., Mara, T., Fahs, M., Grunberger, O., Ackerer, P., 2017. Hydraulic and transport parameter assessment using column infiltration experiments. Hydrology and Earth System Sciences 21, 2263–2275. URL: https://www.hydrol-earth-syst-sci.net/21/2263/2017/, doi:10.5194/hess-21-2263-2017.

Zou, Z.Y., Young, M., Li, Z., Wierenga, P., 2001. Estimation of depth averaged unsaturated soil hydraulic properties from infiltration experiments. Journal of Hydrology 242, 26 – 42. URL: http://www.sciencedirect.com/science/article/pii/S0022169400003851, doi:http://dx.doi.org/10.1016/S0022-1694(00)00385-1.